

Scattering of flexural wave in a thin plate with multiple inclusions by using the null-field integral equation approach

Wei-Ming Lee¹, Jeng-Tzong Chen², Rui-En Jiang¹

¹ Department of Mechanical Engineering, China Institute of Technology, Taipei, Taiwan

² Department of Harbor and River Engineering, National Taiwan Ocean University, Keelung, Taiwan

E-mail:wmlee@cc.chit.edu.tw jtchen@mail.ntou.edu.tw

Abstract

The subject of scattering flexural wave in a thin plate with multiple inclusions subject to the incident wave is studied in this paper. A semi-analytical approach is proposed to solve this problem which can be decomposed into several internal inclusion problems and an external plate problem under the incident wave. The intensity of radiation field in the associated external problem can be derived by using the null-field integral formulation. The dynamic moment concentration factor (DMCF) around the circular inclusions, as well as the far field scattering pattern is determined. The numerical results for an infinite plate with one inclusion are compared with the available analytical solutions to verify the validity of the proposed method. For the cases of small wave number, the quasi-static results of an infinite plate with one or multiple circular inclusions are compared with static data of finite element method (FEM) using ABAQUS. Numerical results indicate that the DMCF of two inclusions is apparently larger than that of one when two inclusions are close to each other. Fictitious frequency appearing in the external problem can be suppressed by using the more number of Fourier series terms. The effects of space between inclusions on both the DMCF and the far scattering pattern are also investigated. It shows that the space between scatters has the opposite effect on the near field in comparison with the far field.

Keywords: scattering, flexural wave, dynamic moment concentration, far field scattering pattern, null-field boundary integral equation

1. Introduction

Plates with multiple circular inclusions are commonly observed in engineering structures. These inclusions, or inhomogeneous materials, usually take place in shapes of discontinuity such as thickness reduction, due to corrosion, or strength degradation, to

delamination. Dynamic loadings under the circumstance always result in stress concentration with ensuing loading capacity reduction and fatigue failure.

The deformation and corresponding stresses induced by dynamic force are inducted throughout the structure by means of wave propagation. At the near field of the inhomogeneity i.e., scatter, flexural wave reflected in all directions recursively interacts with the incident wave. It turns out that the scattering of the stress wave results in dynamic stress concentration [1]. On the other hand, certain applications of the far field scattering flexural response can be obtained in vibration analysis or structural health-monitoring system.

Nishimura and Jimbo [2] are two pioneer investigators to analytically study dynamic stress concentration. They calculated the stresses in the vicinity of a spherical inclusion in the elastic solid under harmonic force. Pao [3] studied the scattering of flexural waves and dynamic stress concentrations around a circular hole, and proposed an analytical solution. Since then, most research has focused on the scattering of elastic wave and dynamic stress concentration and has led to a rapid development of analytical or numerical approach such as wave function expansion method, complex variable method, boundary integral equation method (BIEM) and boundary element method (BEM) [1].

Leviatan *et al.* [4] presented a source-model technique for the analysis of the scattering of a time-harmonic flexural wave in a thin elastic plate by a small patch made of material other than that of the plate. However, the fictitious sources are located at a certain distance away from the boundary of the patch. By using the flux conservation relation and optical theorem, Norris *et al.* [5] considered the scattering of flexural waves by circular inclusions with different plate properties and obtained numerical results. Squire *et al.*

[6] applied the wave function expansion method to study the scattering properties of a single coated cylindrical anomaly located in a thin plate on which flexural waves propagate. Wang [7] presented a theoretical and experimental investigation of the scattering behavior of extensional and flexural plate waves by a cylindrical inhomogeneity. Peng [8] investigated flexural wave scattering and dynamic stress concentration in a heterogeneous plate with multiple cylindrical patches by using acoustical wave propagator technique. The predicted result of the principal stress was compared with the exact analytical solution in a thin plate without patches. Nevertheless, predicted results of dynamic stress concentration were not verified by any independent method. Recently, one monograph is devoted to discussing the multiple scattering in acoustics, electromagnetism, seismology and hydrodynamics [9].

From literature reviews stated previously, few papers except [8] have been published to date reporting the scattering of flexural wave in plate with more than one inclusion. Recently, we proposed a semi-analytical null-field integral equation method for eigensolution of a circular plate with multiple circular holes [10]. The advantage of this approach is employing the degenerate kernel to avoid calculating principal values, which is of great difficulties in the case of plate. The introduction of degenerate kernel in companion with Fourier series was proved to yield the exponential convergence [11] instead of the linear algebraic convergence in BEM. Furthermore, Kobayashi and Nishimura [12] pointed out that the integral equation method seems to be most effective to deal with two-dimensional steady-state flexural wave problems.

This paper extends the null-field integral approach to the external plate problem to solve scattering of flexural waves by multiple circular inclusions in a thin plate. A linear algebraic system can be constructed by uniformly collocating points on the boundary and taking finite terms of Fourier series. The displacement and corresponding section force are calculated by using boundary integral equations for the domain point after determining the Fourier coefficients of unknown boundary density. For the multiply-connected plate problem, the slope (bending angle) and moment in the normal and tangential directions are determined with

scrutiny in the adaptive observer system. Therefore, the operator of transformation matrix for the slope and moment is employed to deal with this problem. The results for an infinite plate with one circular inclusion are compared with the analytical solutions [5, 6] to verify the validity of the proposed method. For the cases of small wave number, the results for multiple inclusions will be compared with those of FEM using ABAQUS [13] to demonstrate the generality of the proposed method. In the end, the effect of central distance between inclusions on the DMCF and the far scattering pattern are also investigated by using the proposed method.

2. Problem statement and boundary integral formulation

2.1 Problem statement

The governing equation of the flexural wave for a uniform infinite thin plate with randomly distributed circular inclusions as shown in Figure 1 is written as follows:

$$\nabla^4 u(x) = k^4 u(x), \quad x \in \Omega \quad (1)$$

where ∇^4 is the biharmonic operator, u is the out-of-plane elastic displacement, $k^4 = \omega^2 \rho_0 h / D$, k (2π /wave length) is the wave number of elastic wave, ω is the circular frequency, ρ_0 is the volume density, $D = Eh^3 / 12(1-\mu^2)$ is the flexural rigidity, E denotes the Young's modulus, μ is the Poisson's ratio, h is the plate thickness and Ω is the domain of the thin plate.

2.2 Boundary integral equation for the collocation point in the domain

The integral representation for the plate problem can be derived from the Rayleigh-Green identity [14] as follows:

$$u(x) = \int_B U(s,x)v(s)dB(s) - \int_B \Theta(s,x)m(s)dB(s) + \int_B M(s,x)\theta(s)dB(s) - \int_B V(s,x)u(s)dB(s) \quad (2)$$

where B is the boundary of the domain Ω , $u(x)$ is the displacement, s and x mean the source and field points, respectively. $U(s,x)$, $\Theta(s,x)$, $M(s,x)$ and $V(s,x)$ in Eqs.(2) are kernel functions. The kernel function $U(s,x)$ in Eq. (2),

$$U(s,x) = \frac{1}{8k^2 D} \left[Y_0(kr) - iJ_0(kr) + \frac{2}{\pi} K_0(kr) \right], \quad (3)$$

is the fundamental solution [14] which satisfies

$$\nabla^4 U(s, x) - k^4 U(s, x) = \delta(s - x) \quad (4)$$

where $\delta(s - x)$ is the Dirac-delta function, $Y_0(kr)$ and $K_0(kr)$ are the zeroth-order of the second-kind Bessel and modified Bessel functions, respectively, $J_0(kr)$ is the zeroth-order of the first-kind Bessel function, $r \equiv |s - x|$ and $i^2 = -1$. The other three kernel functions, $\Theta(s, x)$, $M(s, x)$ and $V(s, x)$, in Eq.(2) can be obtained by applying the following slope, moment and effective shear operators defined by

$$K_\theta = \frac{\partial(\cdot)}{\partial n} \quad (5)$$

$$K_M = -D \left[\mu \nabla^2(\cdot) + (1 - \mu) \frac{\partial^2(\cdot)}{\partial n^2} \right] \quad (6)$$

$$K_V = -D \left[\frac{\partial}{\partial n} \nabla^2(\cdot) + (1 - \mu) \frac{\partial}{\partial t} \left(\frac{\partial}{\partial n} \frac{\partial(\cdot)}{\partial t} \right) \right] \quad (7)$$

to the kernel $U(s, x)$ with respect to the source point, where $\partial/\partial n$ and $\partial/\partial t$ are the normal and tangential derivatives, respectively, ∇^2 means the Laplacian operator.

2.3 Null-field integral equations

The null-field integral equations regarding displacement and slope can be derived from boundary integral equation and by collocating the field point outside the domain. They are expressed as follows:

$$0 = \int_B U(s, x) v(s) dB(s) - \int_B \Theta(s, x) m(s) dB(s) + \int_B M(s, x) \theta(s) dB(s) - \int_B V(s, x) u(s) dB(s) \quad (8)$$

$$0 = \int_B U_\theta(s, x) v(s) dB(s) - \int_B \Theta_\theta(s, x) m(s) dB(s) + \int_B M_\theta(s, x) \theta(s) dB(s) - \int_B V_\theta(s, x) u(s) dB(s) \quad (9)$$

where Ω^C is the complementary domain of Ω . It is noted that once kernel functions are expressed in proper degenerate forms, which will be described in the next subsection, the collocation points can be exactly located on the real boundary, that is $x \in \Omega^C \cup B$.

2.4 Degenerate kernels and Fourier series for boundary densities

In the polar coordinates, the field point and source point can be expressed as (ρ, ϕ) and (R, θ) , respectively. By employing the addition theorem [15], the kernel function $U(s, x)$ is expanded in the series form as follows:

$$U^I(s, x) = \frac{1}{8k^2} \sum_{m=0}^{\infty} \varepsilon_m \{ J_m(k\rho) Y_m(kR) + \frac{2}{\pi} I_m(\lambda\rho) K_m(kR) \} \cos[m(\theta - \phi)], \rho < R \quad (10)$$

$$U^E(s, x) = \frac{1}{8k^2} \sum_{m=0}^{\infty} \varepsilon_m \{ J_m(kR) Y_m(k\rho) + \frac{2}{\pi} I_m(kR) K_m(k\rho) \} \cos[m(\theta - \phi)], \rho \geq R$$

where ε_m is the Neumann factor ($\varepsilon_m = 1, m=0$; $\varepsilon_m = 2, m=1, 2, \dots, \infty$) and the superscripts "I" and "E" denote the interior and exterior cases for $U(s, x)$ degenerate kernels to distinguish $\rho < R$ and $\rho > R$, respectively as shown in Figure 2. The degenerate kernels $\Theta(s, x)$, $M(s, x)$ and $V(s, x)$ in the null-field boundary integral equations can be obtained by applying the operators of Eqs.(5)-(7) to the degenerate $U(s, x)$ kernel with respect to the source point s .

In order to fully utilize the geometry of circular boundary, the displacement $u(s)$, slope $\theta(s)$, moment $m(s)$ and shear force $v(s)$ along the circular boundaries in the null-field integral equations can be expanded in terms of Fourier series, respectively, as shown below:

$$u(s) = u_{c0} + \sum_{n=1}^M (u_{cn} \cos n\theta + u_{sn} \sin n\theta), \quad s \in B, \quad (11)$$

$$\theta(s) = \theta_{c0} + \sum_{n=1}^M (\theta_{cn} \cos n\theta + \theta_{sn} \sin n\theta), \quad s \in B, \quad (12)$$

$$m(s) = m_{c0} + \sum_{n=1}^M (m_{cn} \cos n\theta + m_{sn} \sin n\theta), \quad s \in B, \quad (13)$$

$$v(s) = v_{c0} + \sum_{n=1}^M (v_{cn} \cos n\theta + v_{sn} \sin n\theta), \quad s \in B, \quad (14)$$

where u_{c0} , u_{cn} , u_{sn} , θ_{c0} , θ_{cn} , θ_{sn} , m_{c0} , m_{cn} , m_{sn} , v_{c0} , v_{cn} and v_{sn} are the Fourier coefficients and M is the number of Fourier series terms.

3 Adaptive observer system and transformation of tensor components

Consider an infinite thin plate with multiple circular inclusions as shown in Fig. 1. Since the direct boundary integral equations are frame indifferent (*i.e.* rule of objectivity), the origin of the observer system can be adaptively located on the center of each circle under integration. Figure 3 shows the circular boundary integration in the adaptive observer system. The dummy variable in the circular contour integration is the angle (θ) instead of radial coordinate (R). By using the orthogonal property between degenerated kernels and Fourier series in adaptive system, all the improper

boundary integrals in Eqs.(8)-(9) can be transformed to series sum and then be determined analytically free of principal value sense.

For the case of multiple inclusions, it is inevitable that the source and field points locate on different circular boundaries. The calculated boundary data such as the slope, moment and effective shear force should be transformed to the direction where the specified boundary conditions are given. As shown in Figure 4, ϕ_i is the angle of the collocation point x_i with respect to o_i , which is center of the circle under integration, ϕ_c is that with respect to o_j , which is center of the circle on which collocation point is located. According to the transformation law for the components of tensor, we have

$$\begin{bmatrix} (\cdot)_n \\ (\cdot)_t \end{bmatrix} = \begin{bmatrix} \cos(\delta) & \sin(\delta) \\ -\sin(\delta) & \cos(\delta) \end{bmatrix} \begin{bmatrix} (\cdot)_r \\ (\cdot)_\theta \end{bmatrix}, \quad (15)$$

$$\begin{bmatrix} (\cdot)_{nn} \\ (\cdot)_{nt} \\ (\cdot)_{tt} \end{bmatrix} = \begin{bmatrix} \cos^2(\delta) & \sin^2(\delta) & 2\sin(\delta)\cos(\delta) \\ \sin^2(\delta) & \cos^2(\delta) & -2\sin(\delta)\cos(\delta) \\ -\sin(\delta)\cos(\delta) & \sin(\delta)\cos(\delta) & \cos^2(\delta) - \sin^2(\delta) \end{bmatrix} \begin{bmatrix} (\cdot)_{rr} \\ (\cdot)_{\theta\theta} \\ (\cdot)_{r\theta} \end{bmatrix}, \quad (16)$$

Based on Equations (15) and (16), the general rotated slope, normal bending and tangential bending moment kernels can be obtained by following operators:

$$K_\theta^R = \cos(\delta) \frac{\partial(\cdot)}{\partial n} + \sin(\delta) \frac{\partial(\cdot)}{\partial t} \quad (17)$$

$$K_n^R = -D \left\{ \left[\mu + (1-\mu)\sin^2(\delta) \right] \nabla^2(\cdot) + \cos(2\delta)(1-\mu) \frac{\partial^2(\cdot)}{\partial n^2} + \sin(2\delta)(1-\mu) \frac{\partial}{\partial n} \left(\frac{\partial(\cdot)}{\partial t} \right) \right\} \quad (18)$$

$$K_t^R = -D \left\{ \left[\mu + (1-\mu)\cos^2(\delta) \right] \nabla^2(\cdot) + \cos(2\delta)(\mu-1) \frac{\partial^2(\cdot)}{\partial n^2} - \sin(2\delta)(1-\mu) \frac{\partial}{\partial n} \left(\frac{\partial(\cdot)}{\partial t} \right) \right\} \quad (19)$$

where $\delta = \phi_c - \phi_i$. When the angle ϕ_c equals to the angle ϕ_i or the angle difference δ equals to zero, Eqs.(17) and (18) are simplified to the Eqs.(5) and (6). The expressions of rotated degenerate kernels, $U_\theta(s,x)$, $\Theta_\theta(s,x)$, $M_\theta(s,x)$, $V_\theta(s,x)$, $U_m(s,x)$, $\Theta_m(s,x)$ and $M_m(s,x)$, can be obtained by applying the operators of Eqs.(17)-(19) to the degenerate kernel $U(s,x)$, $\Theta(s,x)$, $M(s,x)$ and $V(s,x)$ with respect to the field point x .

4 Linear algebraic system

Consider an infinite plate containing H nonoverlapping circular inclusions shown in Figure 3 where o_j ($j=1, 2, \dots, H$) is the position vector of each circular inclusion, R_j denotes the radius of the j th circular region,

x_j is the collocation point on the j th circular boundary and B_j is the boundary of the j th circular inclusion. Since the four null field integral equations [10] in the plate formulation are provided, there are 6 (C_2^4) options of choosing any two equations to solve the problems. For the purpose of computational efficiency, Equations (8) and (9) are used to analyze the plate problem. By uniformly collocating N ($=2M+1$) points on each circular boundary in Eqs. (8) and (9), we have

$$0 = \sum_{j=1}^H \int_{B_j} \{ U(s,x)v(s) - \Theta(s,x)m(s) + M(s,x)\theta(s) - V(s,x)u(s) \} dB_j(s), \quad x \in B, \quad (20)$$

$$0 = \sum_{j=1}^H \int_{B_j} \{ U_\theta(s,x)v(s) - \Theta_\theta(s,x)m(s) + M_\theta(s,x)\theta(s) - V_\theta(s,x)u(s) \} dB_j(s), \quad x \in B. \quad (21)$$

In the B_j integration, the origin of the observer system is adaptively located at the center o_j from which the degenerate kernels and Fourier series are described. The selection of interior or exterior degenerate kernel depends on $\rho < R$ or $\rho > R$, respectively, according to the observer system. By using orthogonal property, a linear algebraic system can be written as follows:

$$\begin{bmatrix} U^{11} & -\Theta^{11} & U^{12} & -\Theta^{12} & \dots & U^{1H} & -\Theta^{1H} \\ U_\theta^{11} & -\Theta_\theta^{11} & U_\theta^{12} & -\Theta_\theta^{12} & \dots & U_\theta^{1H} & -\Theta_\theta^{1H} \\ U^{21} & -\Theta^{21} & U^{22} & -\Theta^{22} & \dots & U^{2H} & -\Theta^{2H} \\ U_\theta^{21} & -\Theta_\theta^{21} & U_\theta^{22} & -\Theta_\theta^{22} & \dots & U_\theta^{2H} & -\Theta_\theta^{2H} \\ \vdots & \vdots & \vdots & \vdots & \ddots & \vdots & \vdots \\ U^{H1} & -\Theta^{H1} & U^{H2} & -\Theta^{H2} & \dots & U^{HH} & -\Theta^{HH} \\ U_\theta^{H1} & -\Theta_\theta^{H1} & U_\theta^{H2} & -\Theta_\theta^{H2} & \dots & U_\theta^{HH} & -\Theta_\theta^{HH} \end{bmatrix} \begin{Bmatrix} v^1 \\ m^1 \\ v^2 \\ m^2 \\ \vdots \\ v^H \\ m^H \end{Bmatrix} = \begin{bmatrix} -M^{11} & V^{11} & -M^{12} & V^{12} & \dots & -M^{1H} & V^{1H} \\ -M_\theta^{11} & V_\theta^{11} & -M_\theta^{12} & V_\theta^{12} & \dots & -M_\theta^{1H} & V_\theta^{1H} \\ -M^{21} & V^{21} & -M^{22} & V^{22} & \dots & -M^{2H} & V^{2H} \\ -M_\theta^{21} & V_\theta^{21} & -M_\theta^{22} & V_\theta^{22} & \dots & -M_\theta^{2H} & V_\theta^{2H} \\ \vdots & \vdots & \vdots & \vdots & \ddots & \vdots & \vdots \\ -M^{H1} & V^{H1} & -M^{H2} & V^{H2} & \dots & -M^{HH} & V^{HH} \\ -M_\theta^{H1} & V_\theta^{H1} & -M_\theta^{H2} & V_\theta^{H2} & \dots & -M_\theta^{HH} & V_\theta^{HH} \end{bmatrix} \begin{Bmatrix} \theta^1 \\ u^1 \\ \theta^2 \\ u^2 \\ \vdots \\ \theta^H \\ u^H \end{Bmatrix} \quad (22)$$

For brevity, a unified form $[U^{ij}]$ ($i=1,2,3,\dots,H$ and $j=1,2,3,\dots,H$) denote the response of $U(s,x)$ kernel at the i th circle point due to the source at the j th circle. Otherwise, the same definition is for $[\Theta^{ij}]$, $[M^{ij}]$, $[V^{ij}]$, $[U_\theta^{ij}]$, $[\Theta_\theta^{ij}]$, $[M_\theta^{ij}]$ and $[V_\theta^{ij}]$ kernels. The explicit expressions for sub-vectors $[u^i]$, $[\theta^i]$, $[m^i]$ and $[v^i]$ can be described as follows:

$$u^i = \begin{Bmatrix} u_{c0}^i \\ u_{c1}^i \\ \vdots \\ u_{cM}^i \\ u_{sM}^i \end{Bmatrix}, \quad \theta^i = \begin{Bmatrix} \theta_{c0}^i \\ \theta_{c1}^i \\ \vdots \\ \theta_{cM}^i \\ \theta_{sM}^i \end{Bmatrix}, \quad m^i = \begin{Bmatrix} m_{c0}^i \\ m_{c1}^i \\ \vdots \\ m_{cM}^i \\ m_{sM}^i \end{Bmatrix}, \quad v^i = \begin{Bmatrix} v_{c0}^i \\ v_{c1}^i \\ \vdots \\ v_{cM}^i \\ v_{sM}^i \end{Bmatrix}. \quad (23)$$

The explicit expressions for the sub-matrices of $[U^j]$, $[\Theta^j]$, $[M^j]$, $[V^j]$, $[U_\theta^j]$, $[\Theta_\theta^j]$, $[M_\theta^j]$ and $[V_\theta^j]$ can be written as shown below:

$$K^j = \begin{bmatrix} K_{0c}^j(\rho_1, \phi_1) & K_{1c}^j(\rho_1, \phi_1) & K_{1s}^j(\rho_1, \phi_1) & \cdots & K_{Ms}^j(\rho_1, \phi_1) \\ K_{0c}^j(\rho_2, \phi_2) & K_{1c}^j(\rho_2, \phi_2) & K_{1s}^j(\rho_2, \phi_2) & \cdots & K_{Ms}^j(\rho_2, \phi_2) \\ \vdots & \vdots & \vdots & \ddots & \vdots \\ K_{0c}^j(\rho_N, \phi_N) & K_{1c}^j(\rho_N, \phi_N) & K_{1s}^j(\rho_N, \phi_N) & \cdots & K_{Ms}^j(\rho_N, \phi_N) \end{bmatrix}_{N \times N} \quad (24)$$

where K can be either one of U , Θ , M , V , U_θ , Θ_θ , M_θ and V_θ . The notations ϕ_k and ρ_k ($k=1,2,3,\dots,N$) shown in Fig. 3 are the angle and radius of the k -th collocation point on the i -th circular boundary with respect to the center of the j -th circular boundary (the origin of the observer system) and the element of the sub-matrices can be determined by

$$K_{0c}^j(\rho_k, \phi_k) = \int_0^{2\pi} K(R_j, \theta_j; \rho_k, \phi_k) \cos(n\theta) (R_j d\theta_j), \quad n=0,1,2,\dots,M, \quad (25)$$

$$K_{1s}^j(\rho_k, \phi_k) = \int_0^{2\pi} K(R_j, \theta_j; \rho_k, \phi_k) \sin(n\theta) (R_j d\theta_j), \quad n=1,2,\dots,M \quad (26)$$

5 Techniques for solving scattering problems of inclusions

For an infinite thin plate with multiple inclusions subject to incident flexural wave, the systems for surrounding plate, or matrix, and each inclusion can be represented, respectively, as

$$\begin{bmatrix} U^{M_j} & -\Theta^{M_j} \\ U_\theta^{M_j} & -\Theta_\theta^{M_j} \end{bmatrix} \begin{Bmatrix} v_j^r \\ m_j^r \end{Bmatrix} + \begin{bmatrix} M^{M_j} & -V^{M_j} \\ M_\theta^{M_j} & -V_\theta^{M_j} \end{bmatrix} \begin{Bmatrix} \theta_j^r \\ u_j^r \end{Bmatrix} = 0 \quad (27)$$

$$\begin{bmatrix} U^{I_j} & -\Theta^{I_j} \\ U_\theta^{I_j} & -\Theta_\theta^{I_j} \end{bmatrix} \begin{Bmatrix} v_j \\ m_j \end{Bmatrix} + \begin{bmatrix} M^{I_j} & -V^{I_j} \\ M_\theta^{I_j} & -V_\theta^{I_j} \end{bmatrix} \begin{Bmatrix} \theta_j \\ u_j \end{Bmatrix} = 0 \quad (28)$$

where the subscript j denotes the j th inclusion; the superscript M and I denote the matrix and inclusion, respectively; the superscript r denotes radiation from the boundary of the matrix. The displacement u_j , slope θ_j , moment m_j and shear force v_j are continuous across each circular interface B_j . For the scattering problem, it can be further decomposed into two parts, (a) incident wave field and (b) radiation field, as shown in Fig. 5. For satisfying the boundary continuity conditions, the radiation boundary condition in part (b) is

$$u_j^r = u_j - u_j^i \quad (29)$$

$$\theta_j^r = \theta_j - \theta_j^i \quad (30)$$

$$m_j^r = m_j - m_j^i \quad (31)$$

$$v_j^r = v_j - v_j^i \quad (32)$$

where the subscript i denotes the incidence part. By substituting Equations (29)-(32) into Eq. (27) and then combining with Eq.(28), the system for an infinite plate containing two inclusions, for instance, can be represented as

$$\begin{bmatrix} U^{M_{11}} & -\Theta^{M_{11}} & M^{M_{11}} & -V^{M_{11}} & U^{M_{12}} & -\Theta^{M_{12}} & M^{M_{12}} & -V^{M_{12}} \\ U_\theta^{M_{11}} & -\Theta_\theta^{M_{11}} & M_\theta^{M_{11}} & -V_\theta^{M_{11}} & U_\theta^{M_{12}} & -\Theta_\theta^{M_{12}} & M_\theta^{M_{12}} & -V_\theta^{M_{12}} \\ U^{I_1} & -\Theta^{I_1} & M^{I_1} & -V^{I_1} & 0 & 0 & 0 & 0 \\ U_\theta^{I_1} & -\Theta_\theta^{I_1} & M_\theta^{I_1} & -V_\theta^{I_1} & 0 & 0 & 0 & 0 \\ U^{M_{21}} & -\Theta^{M_{21}} & M^{M_{21}} & -V^{M_{21}} & U^{M_{22}} & -\Theta^{M_{22}} & M^{M_{22}} & -V^{M_{22}} \\ U_\theta^{M_{21}} & -\Theta_\theta^{M_{21}} & M_\theta^{M_{21}} & -V_\theta^{M_{21}} & U_\theta^{M_{22}} & -\Theta_\theta^{M_{22}} & M_\theta^{M_{22}} & -V_\theta^{M_{22}} \\ 0 & 0 & 0 & 0 & U^{I_2} & -\Theta^{I_2} & M^{I_2} & -V^{I_2} \\ 0 & 0 & 0 & 0 & U_\theta^{I_2} & -\Theta_\theta^{I_2} & M_\theta^{I_2} & -V_\theta^{I_2} \end{bmatrix} \begin{Bmatrix} v_1 \\ m_1 \\ \theta_1 \\ u_1 \\ v_2 \\ m_2 \\ \theta_2 \\ u_2 \end{Bmatrix} = \begin{Bmatrix} f_1^r \\ f_1^m \\ 0 \\ 0 \\ f_2^r \\ f_2^m \\ 0 \\ 0 \end{Bmatrix} \quad (33)$$

$$f_1^r = U^{M_{11}} v_1^i - \Theta^{M_{11}} m_1^i + M^{M_{11}} \theta_1^i - V^{M_{11}} u_1^i + U^{M_{13}} v_3^i - \Theta^{M_{13}} m_3^i + M^{M_{13}} \theta_3^i - V^{M_{13}} u_3^i \quad (30)$$

$$f_1^m = U_\theta^{M_{11}} v_1^i - \Theta_\theta^{M_{11}} m_1^i + M_\theta^{M_{11}} \theta_1^i - V_\theta^{M_{11}} u_1^i + U_\theta^{M_{13}} v_3^i - \Theta_\theta^{M_{13}} m_3^i + M_\theta^{M_{13}} \theta_3^i - V_\theta^{M_{13}} u_3^i \quad (31)$$

$$f_2^r = U^{M_{21}} v_1^i - \Theta^{M_{21}} m_1^i + M^{M_{21}} \theta_1^i - V^{M_{21}} u_1^i + U^{M_{23}} v_3^i - \Theta^{M_{23}} m_3^i + M^{M_{23}} \theta_3^i - V^{M_{23}} u_3^i \quad (32)$$

$$f_2^m = U_\theta^{M_{21}} v_1^i - \Theta_\theta^{M_{21}} m_1^i + M_\theta^{M_{21}} \theta_1^i - V_\theta^{M_{21}} u_1^i + U_\theta^{M_{23}} v_3^i - \Theta_\theta^{M_{23}} m_3^i + M_\theta^{M_{23}} \theta_3^i - V_\theta^{M_{23}} u_3^i \quad (34)$$

After calculating the displacement, slope, moment and effective shear force along the boundary, the radiation field can be solved by employing the boundary integral equation for the domain point. The scattering field is determined by superimposing radiation field and incident field. The tangential bending moment $M_t(x)$ can be determined by applying the operator of Eq.(19) to the resulted scattering field with respect to the field point.

5.1 Dynamic moment concentration factor

An incident flexural wave is represented by $u_0^{(i)} e^{ik(x \cos(\phi_0) + y \sin(\phi_0))}$ (35)

where $u_0^{(i)}$ is the amplitude of incident wave, k is the wave number and ϕ_0 is the incident angle. Under the polar coordinates, the bending moment and effective shear force induced by the incident wave can be determined by substituting Eq. (43) into Eqs.(6) and (7). By setting the amplitude of incident wave $u_0^{(i)} = 1$, the amplitude of moment produced by the incident wave is

$$M_0 = Dk^2 \quad (36)$$

The dynamic moment concentration factor (DMCF) can be determined as

$$DMCF = M_t / M_0 \quad (37)$$

5.2 The scattered far field amplitude

For the most part of scattering applications, it is

interesting to measure the scattered field far away from the scatter. On the other hand, the asymptotic behavior or uniqueness of fundamental solutions (or kernel functions) is an important issue for the numerical computation. Therefore, we examine the behavior of the scattered response in the far field. The scattered far field amplitude $f(\theta)$ [5] in our approach is defined as

$$f(\theta) = \lim_{\rho \rightarrow \infty} \sqrt{2\rho/a} \cdot u^r(\rho) \quad (38)$$

where $u^r(\rho)$ is the out-of-plane elastic displacement of radiation field, ρ is the radius of the field point and a is the radius of inclusion.

6 Numerical results and discussions

The following numerical simulation utilizes the proposed method for finding dynamic moment concentration factor (DMCF) around circular inclusions as well as the far field scattered amplitude. For the cases of small wave number, the same plate problem is independently solved by using FEM (the ABAQUS software) for comparison. In all cases, the thickness of plate is 0.002m unless otherwise specified. The general-purpose triangular shell element, S3, of ABAQUS was used to model the plate element. According to theoretical manual of ABAQUS [13], these elements do not suffer from transverse shear locking even though the thickness of the plate is merely 0.002 m.

An infinite plate with one inclusion of radius a , as shown in Fig. 6, subject to incident flexural wave with $\phi_0 = 0$ was firstly considered. Figure 7 shows the DMCF on the circular boundary, at $\pi/2$, versus the dimensionless wave number by using different number of terms of Fourier series. It indicates that the required number of terms to convergence increases as the incident wave number becomes larger.

In the limit of zero wave number [1] like $ka = 0.005$, the excitation of incident wave is equivalent to the static loading with moment $M_{xx} = M_0$ and $M_{yy} = \nu M_0$ at the four sides. For comparison, a $16m \times 16m$ plate containing one inclusion with radius 1m subject to static bending moments, $M_{xx} = 1.0$ and $M_{yy} = 0.3$ at the four sides was considered in the FEM model where 32138 triangle elements was generated. Figures 8(a) and 8(b) show the polar plot of dynamic moment concentration factors on the circular boundary of the

matrix and inclusion, respectively, by using the present method and FEM. Good agreements can be observed.

Figure 9 shows the far field scattering patterns for a flexible inclusion with $h_1 = h/2$ at dimensionless wave numbers $ka = 0.1, 1.0, 3.0$ and 5.0 . As ka increases, the scattering pattern inclines toward forward scattering and the associated scattering amplitude also get increasing. Figure 10 shows the far field backscattering amplitude versus the dimensionless wave number. The surrounding plate is steel of thickness 0.025m and solid line stands for hole, dash line for rigid inclusion and dash-dot line for inclusion with thickness 0.0125m. The rigid inclusion means the clamped boundary condition around the circular boundary. The proposed results shown in figure 10 match well with those reported in [5]. It can be found that the amplitude for the radiation (or scattering) response in the far field is $O(\rho^{-1/2})$ to satisfy the radiation condition.

To demonstrate the flexural scattering by multiple inclusions, two identical inclusions were considered in Figure 11, where L is the central distance. In the following simulation, the dimensionless central distance L/a will be used. For $L/a = 2.1$, Figure 12 shows the DMCF on the upper circular boundary of inclusion, at $-\pi/2$, versus the dimensionless wave number by using different number of Fourier series terms. The results using fewer Fourier series terms such as $M = 4, 6$ show some peaks at $ka = 3.2, 4.6$. They are found to be identical to the true eigenvalues, 3.196, 4.610 [16], of the clamped circular plate with radius equaling to that of the inclusion. Actually they are the so-called fictitious frequencies of the external problem. It demonstrates that the increasing number of Fourier series terms can suppress the appearance of fictitious frequencies.

For $L/a = 2.1$, figure 13 shows the distribution of DMCF on the upper circular boundary, including plate and inclusion, by using both the present method and FEM. It indicates that the maximum DMCF is larger than that of one, as shown in Figure 8, due to the narrow space between two inclusions. Figures 14 and 15 show the far field scattering patterns for two flexible inclusions with $h_1 = h/2$ and $L/a = 2.1, 10.0$, respectively, at $ka = 0.1, 1.0, 3.0$ and 5.0 . After comparing with the results of one inclusion presented in Figure 9, the far field scattering amplitude of two inclusions is more or

less twice as large as that of one. In addition, the associated fluctuation along the angular direction of two inclusions is more evident than that of only one. Moreover, this trend becomes obvious as the dimensionless central distance increases.

In summary, the space between scatters has the different effect on the near field and the far field, respectively. Specifically, the near field quantity, such as DMCF, increases as L/a decreases, as shown in figure 13, but the fluctuation of the far field scattering along the angular direction becomes evident when L/a increases, as shown in Figures 14 and 15. It implies that the multiple scattering can be simplified by using the single-scattering approximation in studying the near field problem when the spacing between scatters is large enough but the far field study can not follow this rule.

7 Concluding remarks

A semi-analytical approach to solve the problem of flexural wave scattering from multiple inclusions in an infinite thin plate was presented. Our studies focus on the issues of DMCF around the circular inclusion and the far field scattering pattern. Multiple scattering solution was derived by using the superposition technique and the null-field integral equation approach. The advantage of using the degenerate kernels is free of calculating the improper integrals by using principal values in the traditional boundary integral formulation. For an infinite plate with one inclusion, good agreement between the present method and analytical solution is observed. For the cases of small wave number, the proposed results for a plate with one or multiple circular inclusions match well with the static results from finite element method (FEM). Numerical results indicate that DMCF of two inclusions is apparently larger than that of one when two inclusions are close to each other. Moreover it indicates that the space between two inclusions has different effects on the near field and the far field. It is helpful for further study on the multiple scattering. Fictitious frequency of external problem can be suppressed by using the more number of Fourier series terms. As seen from the numerical results, the proposed method provides a semi-analytical solution for the problem of scattering flexural wave by multiple circular inclusions in an infinite thin plate subject to the incident wave, since its

analytical solution is not yet available to date.

References

- [1] Y.H. Pao, C.C. Mow, *Diffraction of elastic waves and dynamics stress concentration*, Crane-Russak, New York, 1972.
- [2] G. Nishimura, Y. Jimbo, A dynamical problem of stress concentration. *Journal of the Faculty of Engineering*, University of Tokyo, Japan, 24 (1955) 101.
- [3] Y.H. Pao, Dynamical stress concentration in an elastic plate, *Transactions of the ASME Journal of Applied Mechanics* (1962) 299-305.
- [4] Y. Leviatan, E.T. Erez, M.J. Beran, A source-model technique for analysis of flexural wave scattering in a heterogeneous thin plate, *The Quarterly Journal of Mechanics and Applied Mathematics* 45 (1992) 499-514,
- [5] A.N. Norris, C. Vemula, Scattering of flexural waves on thin plates, *Journal of Sound and Vibration* 181 (1995) 115-125.
- [6] V. A. Squire, T. W. Dixon, Scattering of flexural waves from a coated cylindrical anomaly in a thin plate, *Journal of Sound and Vibration* 236(2) (2000) 367-373.
- [7] C.H. Wang, F.K. Chang, Scattering of plate waves by a cylindrical inhomogeneity, *Journal of Sound and Vibration* 282 (2005) 429-451.
- [8] S.Z. Peng, Flexural wave scattering and dynamic stress concentration in a heterogeneous plate with multiple cylindrical patches by acoustical wave propagator technique, *Journal of Sound and Vibration* 286 (2005) 729-743.
- [9] P.A. Martin, *Multiple scattering interaction of time-harmonic wave with N obstacles*, Cambridge University Press, Cambridge, 2006.
- [10] W.M. Lee, J.T. Chen, Null-field integral equation approach for free vibration analysis of circular plates with multiple circular holes, *Computational Mechanics* 42 (2008) 733-747.
- [11] R. Kress, *Linear integral equations*, Springer, New York, 1989.
- [12] S. Kobayashi, N. Nishimura, Transient Stress Analysis of Tunnels and Caverns of Arbitrary Shape Due to Traveling Waves. in: *Developments in Boundary Element Methods-II*, Banerjee, P. K., and Shaw, R. P., eds.,

Applied Science, London, 1981, 177-210.

- [13] ABAQUS 6.5 Hibbitt, Karlsson and Sorensen, Inc. RI. 2004.
- [14] M. Kitahara, *Boundary integral equation methods in eigenvalue problems of elastodynamics and thin plates*, Elsevier, Amsterdam, 1985.
- [15] G.N. Watson, *A treatise on the theory of Bessel Functions*, second edition. Cambridge: Cambridge Library edition, 1995.
- [16] A.W. Leissa, *Vibration of plates*, NASA SP-160, 1969.

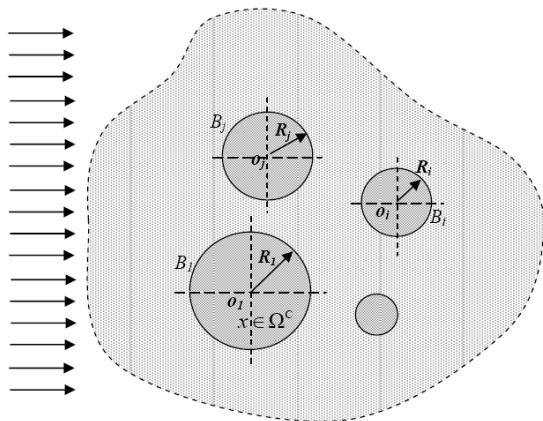


Figure 1 Problem statement for an infinite plate containing multiple circular inclusions subject to an incident flexural wave

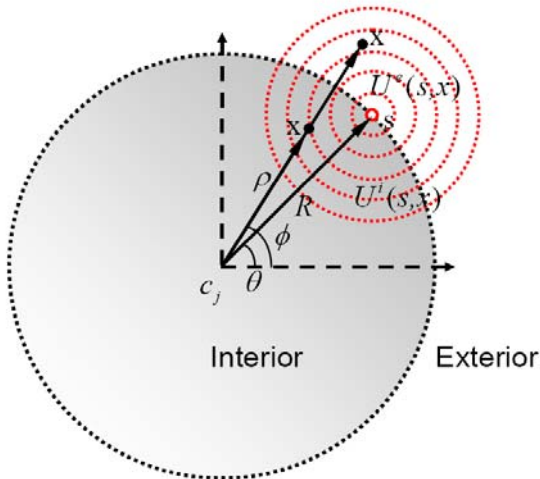


Figure 2 Degenerate kernel for $U(s,x)$

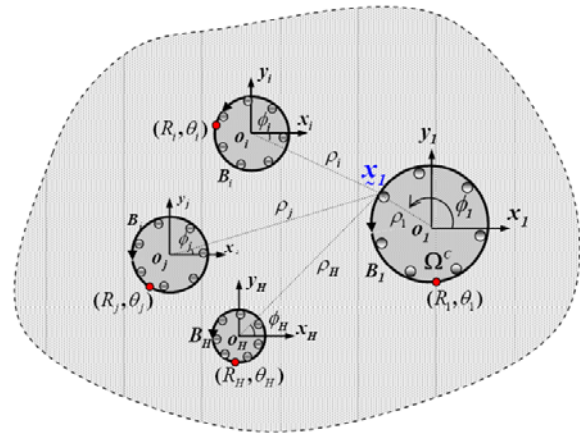


Figure 3 Collocation point and boundary contour integration in the boundary integral equation for the plate by using the adaptive observer system

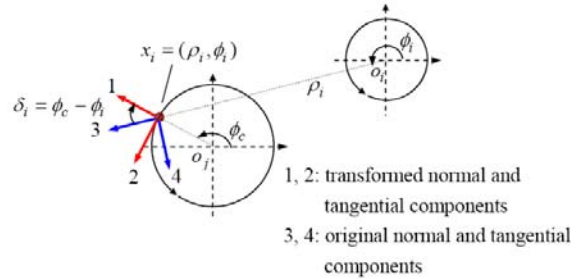


Figure 4 Transformation of tensor components

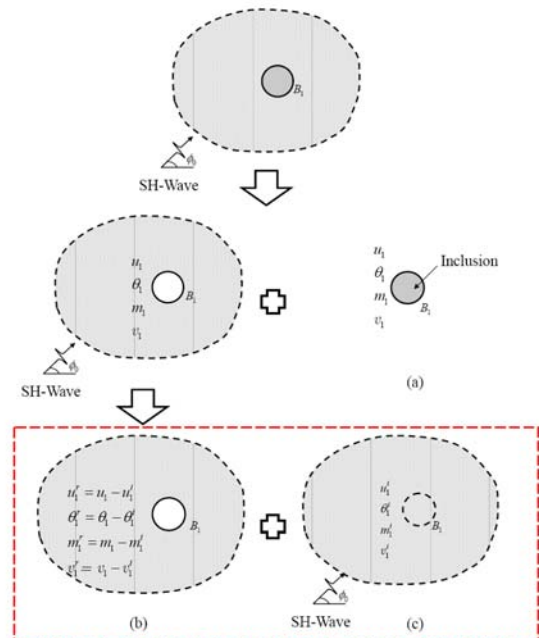


Figure 5 Decomposition of scattering plate problem with an inclusion into (a) an internal inclusion problem (b) an external radiation plate problem (c) incident wave field

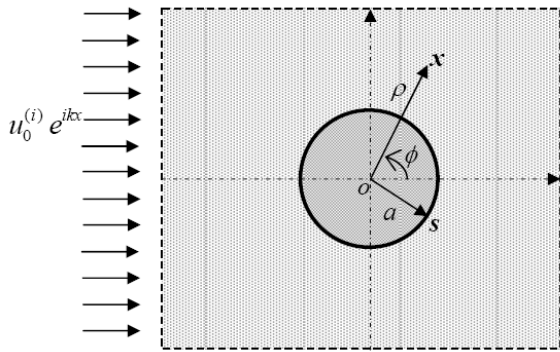


Figure 6 An infinite plate containing an inclusion subject to an incident flexural wave

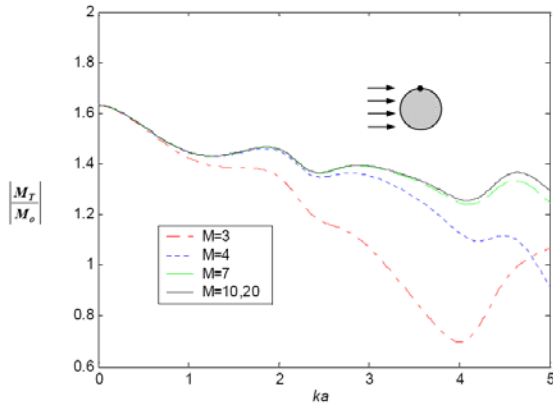


Figure 7 Dynamic moment concentration factor on the circular boundary ($\theta = \pi/2$) versus the dimensionless wave number by using different number of terms of Fourier series

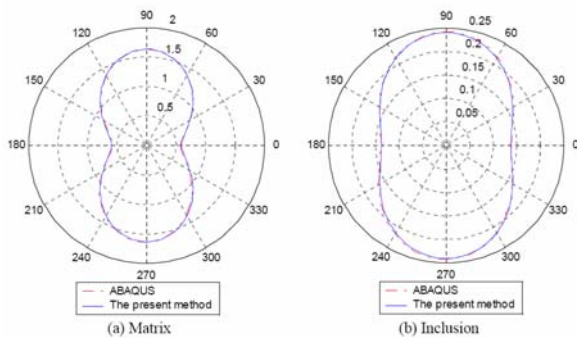


Figure 8 Distribution of dynamic moment concentration factors on the circular boundary of the matrix and inclusion by using the present method ($M=4, ka=0.005$) and FEM (ABAQUS, under equivalent static loading)

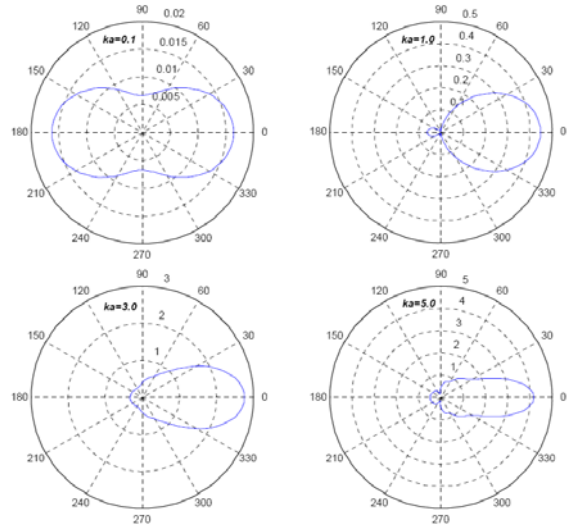


Figure 9 Far field scattering pattern for a flexible inclusion with $h_1=h/2$ at dimensionless wave numbers $ka = 0.1, 1.0, 3.0$ and 5.0

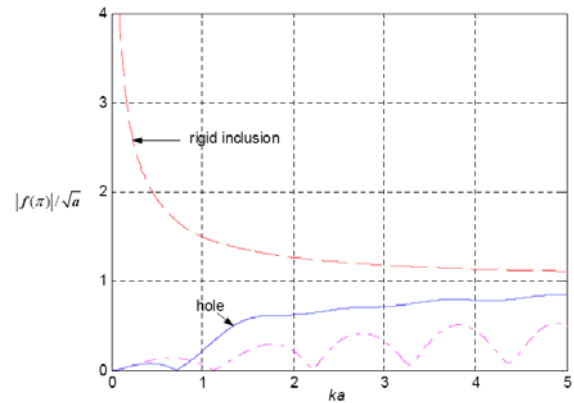


Figure 10 Far field backscattering amplitude versus the dimensionless wave number. The surrounding plate is steel of thickness 0.025m, solid line for the hole, dashed line for the rigid inclusion and dash-dot line for the inclusion with thickness 0.0125m.

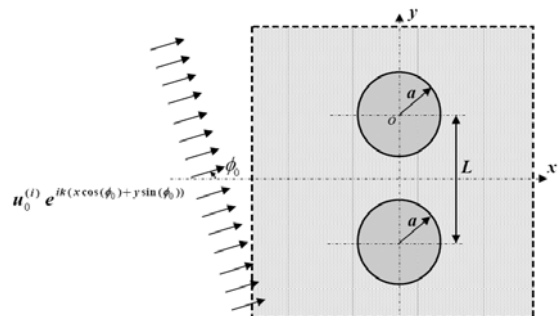


Figure 11 An infinite plate containing two inclusions subject to an incident flexural wave with an incident angle ϕ_0

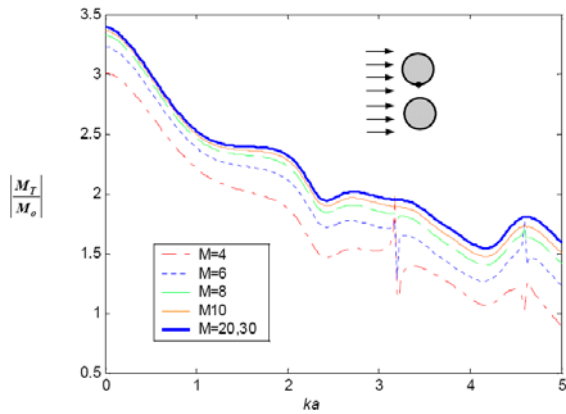


Figure 12 DMCF on the upper circular boundary ($\theta = -\pi/2$) versus the dimensionless wave number by using different number of terms of Fourier series ($L/a = 2.1$)

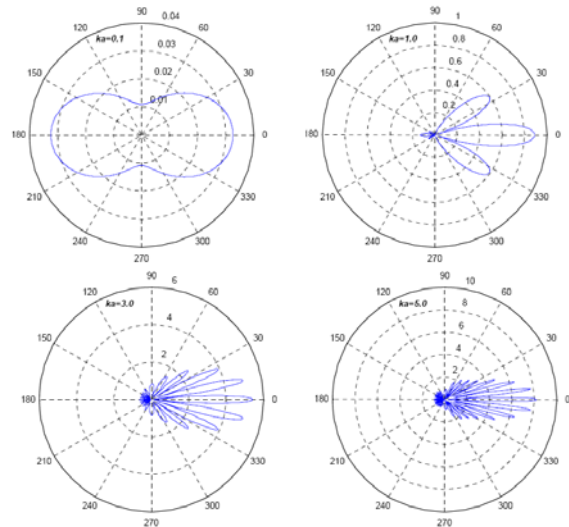


Figure 15 Far field scattering pattern for two flexible inclusions with $h_1=h/2$ and $L/a=10.0$ at dimensionless wave numbers $ka = 0.1, 1.0, 3.0$ and 5.0

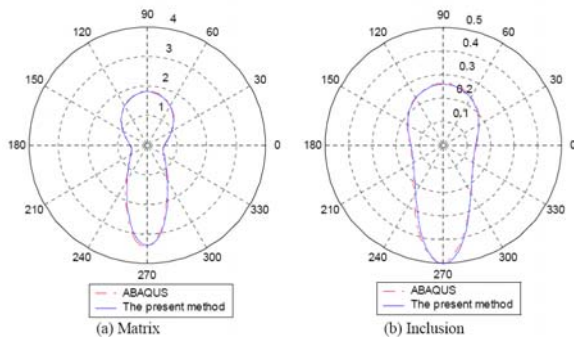


Figure 13 Distribution of dynamic moment concentration factors on the upper circular boundary of the matrix and inclusion by using the present method and FEM ($L/a = 2.1$)

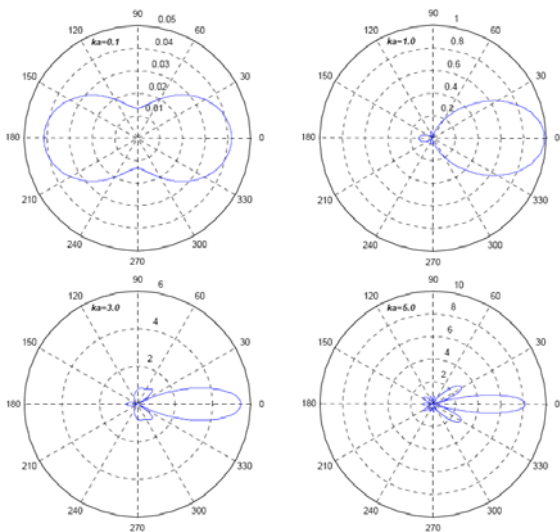


Figure 14 Far field scattering pattern for two flexible inclusions with $h_1=h/2$ and $L/a=2.1$ at dimensionless wave numbers $ka = 0.1, 1.0, 3.0$ and 5.0